Novel sst_4-Selective Somatostatin (SRIF) Agonists. 4. Three-Dimensional Consensus Structure by NMR

Christy Rani R. Grace,[†] Steven C. Koerber,[‡] Judit Erchegyi,[‡] Jean Claude Reubi,[§] Jean Rivier,*[,‡] and Roland Riek[†]

Structural Biology Laboratory and The Clayton Foundation Laboratories for Peptide Biology, The Salk Institute for Biological Studies, 10010 North Torrey Pines Road, La Jolla, California 92037, and Division of Cell Biology and Experimental Cancer Research, Institute of Pathology, University of Berne, CH-3012 Berne, Switzerland

Received May 20, 2003

The three-dimensional NMR structures of eight cyclic octapeptide analogues of somatostatin (SRIF) are described. These analogues, with the basic sequence H-c[Cys^3-Phe^6-Xxx^7-Yyy^8-Lys^9-Thr^{10}-Zzz^{11}-Cys^{14}]-OH (the numbering refers to the position in native SRIF), with Xxx^7 being Phe/Ala/Tyr, Yyy^8 being Trp/DTrp/D-*threo*-β-Me2Nal/L-*threo*-β-Me2Nal, and Zzz^{11} being Phe/Ala, exhibit potent and highly selective binding to human SRIF type 4 (sst_4) receptors. The conformations reveal that the backbones of these analogues do not have the usual type-II′ β-turn reported in the literature for sst_2-subtype-selective analogues. Instead, the structures contain a unique arrangement of side chains of Yyy^8, Lys^9, and Phe^6 or Phe^{11}. The conformational preferences and results from biological analyses of these analogues (parts 1-3 of this series, Rivier et al., Erchegyi et al., and Erchegyi et al., *J. Med. Chem.* **2003**, preceding papers in this issue) allow a detailed study of the structure−activity relationship of SRIF. The proposed consensus structural motif at the binding pocket for the sst_4-selective analogues requires a unique set of distances between an indole/2-naphthyl ring, a lysine side chain, and another aromatic ring. This motif is necessary and sufficient to explain the binding affinities of all of the analogues studied and is distinct from the existing model suggested for sst_2/sst_5 selectivity.

Introduction

Somatostatin (SRIF, H-Ala^1-Gly^2-c[Cys^3-Lys^4-Asn^5-Phe^6-Phe^7-Trp^8-Lys^9-Thr^{10}-Phe^{11}-Thr^{12}-Ser^{13}-Cys^{14}]-OH), a cyclic tetradecapeptide, inhibits the release of several hormones, including growth hormone, glucagon, insulin, secretin, and gastrin.[1,2] It also plays a vital role in neurotransmission and neuromodulation[3,4] and has antiproliferative effects, regulating cell proliferation and differentiation. The diverse biological activities of SRIF are mediated by a family of five different receptors, sst_1−sst_5 (sst's). Due to its broad spectrum of physiological activities and its short duration of action due to rapid proteolytic degradation in vivo,[5] SRIF continues to be a target for the development of small subtype-specific analogues (see refs 6−9 and references therein).

Indeed, over the past three decades, hundreds of SRIF analogues have been reported and tested for their affinity and selectivity toward the five receptor subtypes. Correspondingly, structure−activity relationship (SAR) studies have been initiated that ruled out the specific involvement of the side chains of all residues but Phe^7-DTrp^8-Lys^9-Thr^{10} for biological recognition.[10−12] (Note: The numbering of residues follows that of native SRIF.) Furthermore, extensive structural studies, including NMR and X-ray diffraction,[13] have been carried out to elucidate the pharmacophore and the consensus structural motif of analogues binding predominantly to sst_2/sst_5 (and sst_3) receptors. Veber et al. have demonstrated that the DTrp^8-Lys^9 side chains of the bioactive conformation exist most likely in an equatorial orientation relative to the backbone of the analogue.[14] Kessler and co-workers studied six retro-analogues containing D- or L-Pro in cyclic hexapeptides and showed that the backbone conformation of all the trans-cycloanalogues consists of a β-turn containing the Pro residue in position $i + 1$.[15] Mierke et al. have also concluded that, in the hexapeptide analogues of SRIF, the backbone of the segment Phe-DTrp-Lys-Thr adopts a type-II′ β-turn in DMSO.[16] Goodman and co-workers continued this detailed study on the influence of the bridging region on activity via synthesis and NMR studies of a variety of retro-inverso, stereochemically distinct configurational isomers of this hexapeptide[17] as well as hexapeptides containing acidic and basic peptoid residues.[18,19] They found that the cis isomers adopt a type-II′ β-turn with DTrp^8 in the $i + 1$ position and a type-VIa β-turn with the cis peptide bond of the Phe-Pro linkage. This was further confirmed by several studies, wherein the β-turn motif is observed in GH release-inhibiting analogues and not in analogues with antitumor activity.[20−22]

In contrast, the three-dimensional (3D) structure of a highly sst_2-selective bicylic hexapeptide[23] does not contain a type-II′ β-turn. Cheng et al. reported a type-V′ β-turn in DJS811 which binds with high selectivity to the sst_2 receptor.[24] On the basis of these 3D structures, a bioactive conformation for SRIF analogues binding to sst_2/sst_5 (and sst_3) was established.[18,19,25,26] In this model, the side chains and the relative spatial arrangement of Phe^7, DTrp^8 and Lys^9 constitute the

* To whom correspondence should be addressed. Phone: (858) 453-4100. Fax: (858) 552-1546. E-mail: jrivier@salk.edu.
[†] Structural Biology Laboratory, The Salk Institute for Biological Studies.
[‡] The Clayton Foundation Laboratories for Peptide Biology, The Salk Institute for Biological Studies.
[§] University of Berne.

10.1021/jm030246p CCC: $25.00
Published on Web 11/20/2003

Table 1. sst_1−sst_5 Binding Affinities (IC_{50}, nM) of Analogues Studied by NMR[a]

		IC_{50} (nM)				
no.	compd	sst_1	sst_2	sst_3	sst_4	sst_5
1	H-c[Cys-Phe-Phe-Trp-Lys-Thr-Phe-Cys]-OH	5.3 ± 0.7 (3)	130 ± 65 (3)	13 ± 0.7 (3)	0.7 ± 0.3 (3)	14 ± 4.1 (3)
2	H-c[Cys-Phe-Phe-DTrp-Lys-Thr-Phe-Cys]-OH	27 ± 3.4 (4)	41 ± 8.7 (6)	13 ± 3.2 (4)	1.8 ± 0.7 (4)	46 ± 27 (3)
3	H-c[Cys-Phe-Ala-Trp-Lys-Thr-Phe-Cys]-OH	>1000 (3)	807 ± 146 (3)	750 ± 278 (3)	0.84 ± 0.2 (3)	633 ± 186 (3)
4	H-c[Cys-Phe-Ala-DTrp-Lys-Thr-Phe-Cys]-OH	>1000 (3)	183 ± 18 (3)	897 ± 103 (3)	0.98 ± 0.1 (4)	199 ± 56 (4)
5	H-c[Cys-Phe-Tyr-D-*threo*-β-Me2Nal-Lys-Thr-Phe-Cys]-OH	410 ± 110 (2)	30 ± 0 (2)	18 ± 4 (2)	2.3 ± 1.7 (2)	18 ± 0.5 (2)
6	H-c[Cys-Phe-Tyr-L-*threo*-β-Me2Nal-Lys-Thr-Phe-Cys]-OH	>1000 (5)	194 ± 68 (5)	825 ± 288 (4)	2.8 ± 0.8 (5)	360 ± 213 (4)
7	H-c[Cys-Phe-Ala-Trp-Lys-Thr-Ala-Cys]-OH	>10K (2)	>1000, >10K	>1000, >10K	3.5 (2.8; 4.3)	>1000 (2)
8	H-c[Cys-Phe-Ala-DTrp-Lys-Thr-Ala-Cys]-OH	>10K (2)	>1000, 962	>10K, >1000	9.5 (7.1; 12)	>1000 (2)
9	H-c[DCys-Phe-Tyr-L-*threo*-β-Me2Nal-Lys-Thr-Phe-Cys]-OH	>10K (6)	339 ± 103 (5)	664 ± 81 (5)	3.5 ± 0.5 (6)	668 ± 86 (6)
10	H-c[DCys-Phe-Tyr-D-*threo*-β-Me2Nal-Lys-Thr-Phe-Cys]-OH	545 ± 122 (4)	12 ± 2 (4)	14 ± 3 (4)	0.55 ± 0.03 (3)	27 ± 5.6 (3)
11	H-c[Cys-Phe-LAgl(N$^{\beta}$Me,benzoyl)-Trp-Lys-Thr-Phe-Cys]-OH	>10K (2)	>1000 (2)	403 (500; 305)	5.4 (2.8; 7.9)	>1000 (2)
12	H-c[Cys-Phe-DAgl(N$^{\beta}$Me,benzoyl)-Trp-Lys-Thr-Phe-Cys]-OH	>10K (2)	>1000 (2)	725 (650; 799)	133 (90; 126)	>1000 (2)
13	H-c[Cys-Phe-DAgl(N$^{\beta}$Me,benzoyl)-DTrp-Lys-Thr-Phe-Cys]-OH	>10K (2)	>1000 (2)	>1000 (2)	153 (88; 217)	>1000 (2)
14	H-c[Cys-Phe-LAgl(N$^{\beta}$Me,benzoyl)-DTrp-Lys-Thr-Phe-Cys]-OH	>1000 (3)	460 ± 87 (4)	447 ± 169 (3)	5.2 ± 1.1 (3)	768 ± 129 (3)

[a] The data are obtained from references except for **7** and **8**.[6−8]

most essential elements necessary for binding (see Figure 5C, below). The side chain of DTrp^8 is in close proximity to the side chain of Lys^9 (∼5 Å), whereas the side chain of Phe^7 is about 7−9 Å away from the side chain of DTrp^8 and 9−11 Å from the side chain of Lys^9. To match this pharmacophore motif to the scaffold of a type II′ β-turn, the rotamers of the side chains of DTrp^8 and Phe^7 are in the trans configuration, and that of Lys^9 is in the gauche configuration.

In the preceding papers, we described the synthesis and biological characterization of three families of sst_4-selective SRIF analogues.[6−8] As shown here, members of the first family,[6] exemplified by **11**−**14** (Table 1), were not amenable to NMR investigation in water or DMSO because of the presence of at least two conformers. Whereas members of the second family[7] of sst_4-selective analogues (**5** and **6**, Table 1) could be studied by NMR in DMSO (Tables 2 and 3; Figures 3 and 4), the corresponding DCys^3-containing analogues (**9** and **10**) also showed at least two conformers. Finally, the structures of the parent compounds **1** and **2** and members of the third family[8] (**3** and **4**) were critical for the identification of the consensus structure of sst_4-selective SRIF analogues, which in turn led to the discovery of sst_4-selective analogues with an alanine at position 11 (**7** and **8**). Analogues **2**, **4**, and **8** contain a DTrp at position 8, analogues **1**, **3**, and **7** contain a Trp at position 8, analogues **5** and **10** contain a D-*threo*-β-Me2Nal at position 8, and analogues **6** and **9** contain an L-*threo*-β-Me2Nal at position 8. Furthermore, **3**, **4**, **6**, **7**, **8**, and **9** show highly selective binding to sst_4, while **1**, **2**, **5**, and **10** bind with high affinity to sst_4 as well as to other sst's, except to sst_1 (**5** and **10**). The determination of the 3D structures of **1**−**8** enabled us to propose an sst_4-selective consensus structural motif for SRIF and analogues thereof.

Results

In this section, we present general details about the chemical shift assignment and the structure determination by NMR of each SRIF analogue **1**−**8** shown in Table 1. In addition, some of the features observed in the NMR spectra of **9**−**14** (Table 1) are discussed.

Chemical Shift Assignment, Collection of Structural Restraints, and Structure Determination. The nearly complete chemical shift assignment of proton resonances (Table 2) for analogues **1**−**8** (Table 1) has been carried out using two-dimensional (2D) NMR experiments, using the standard procedure described in the Experimental Section. The N-terminal amino protons for all eight analogues were not observed due to fast exchange with the solvent. Similarly, the amide proton of the second residue, Phe^6, for analogues **1** and **2** could not be detected, probably due to the fast exchange with the solvent. Furthermore, some aromatic ring protons could not be assigned, as shown in Table 2. Chemical shifts can provide insight into the solution structure of peptides, which is particularly true for SRIF analogues. The ring current of the indole ring leads to a distinct shift of the C$^{\gamma}$ protons of the sequential Lys side chain to lower frequencies when these groups are close in space, as in a β-turn. This has been observed in most of the SRIF analogues binding to sst_2, sst_3, and sst_5 receptors, reported in the literature.[16,18,20,22,24,27−31] For the sst_4 analogues studied here, a small upfield shift is observed for the analogues with a DTrp^8 residue (**2**, **4**, **8**) when compared to the analogues having a Trp^8 residue (**1**, **3**, **7**). Similarly, a distinctly large shift is observed for analogue **5**, which has D-*threo*-β-Me2Nal, compared to compound **6**, having L-*threo*-β-Me2Nal. The lack of a distinct chemical shift for Lys protons indicates a different conformation when compared with that of

Table 2. Proton Chemical Shifts of Analogues **1**−**8**[a]

		analogue							
residue	^{1}H	**1**	**2**	**3**	**4**	**5**	**6**	**7**	**8**
Cys[3]	NH								
	αH	3.61	3.58	3.98	4.03	4.06	3.96	3.97	4.05
	*β*H	2.97, 2.41	3.09, 2.54	3.15, 3.06	3.23, 2.90	3.24, 2.87	3.27, 3.00	3.14, 3.03	3.21, 2.87
Phe[6]	NH			8.73	8.61	8.74	8.97	8.71	8.64
	αH	4.29	4.36	4.53	4.52	4.61	4.38	4.53	4.53
	*β*H	2.76, 2.70	2.90, 2.75	2.96, 2.74	3.00, 2.70	2.98, 2.66	2.84, 2.74	2.96, 2.73	3.03, 2.70
	H2,6	6.97	7.06	7.24	7.27	7.19	7.13	7.24	7.27
	H3,5	7.13	7.15	7.39	7.67		7.20		7.68
	H4			7.14	7.02				
		Phe	Phe	Ala	Ala	Tyr	Tyr	Ala	Ala
Phe/Ala/Tyr[7]	NH	8.59	8.24	8.10	8.34	8.27	8.13	8.18	8.35
	αH	4.10	4.38	4.08	4.10	4.55	4.33	4.06	4.12
	*β*H	2.97, 2.80	2.80, 2.71	1.15	1.00	2.72, 2.53	2.81, 2.70	1.15	1.00
	H2,6	7.06	7.18			7.00	6.92		
	H3,5	7.18	7.22			6.63	6.60		
	H4								
		Trp	DTrp	Trp	DTrp	D-*threo*-*β*-Me2Nal	L-*threo*-*β*-Me2Nal	Trp	DTrp
Trp/DTrp/	NH	7.83	8.49	8.01	8.41	8.69	8.03	8.01	8.46
D-*threo*-*β*-Me2Nal/	αH	4.49	4.34	4.37	4.45	4.49	4.62	4.35	4.44
L-*threo*-*β*-Me2Nal[8]	*β*H	3.19, 3.11	3.14, 2.89	3.18, 3.11	3.23, 2.86	3.31	3.47	3.21, 3.14	3.23, 2.88
	H1	10.79	10.74	10.84	10.81	7.68	7.77	10.84	10.82
	H2	7.15	7.10	7.08	7.10	7.41	7.52	7.09	7.11
	H4	7.58	7.53	7.48	7.55	7.79	7.82	7.54	7.55
	H5	6.98	6.97	6.97	6.97	7.83	7.84	6.97	6.97
	H6	7.05	7.04		7.04	7.43	7.44	7.04	7.05
	H7	7.31	7.30	7.29	7.31	7.80	7.82	7.30	7.31
	*γ*H					1.16	1.28		
Lys[9]	NH	8.46	7.95	7.92	7.96	8.08	8.25	7.98	8.00
	αH	4.25	4.34	4.11	4.30	4.01	3.95	4.17	4.31
	*β*H	1.81, 1.49	1.70, 1.47	1.71, 1.53	1.69,1.46	1.47,1.03	1.68, 1.47	1.78,1.59	1.73, 1.49
	*γ*H	1.26	1.30, 1.14	1.16	1.09	0.46	1.02	1.23	1.10
	*δ*H	1.5	1.47	1.47	1.47	1.03	1.38, 1.34	1.51	1.47
	*ϵ*H	2.73	2.73	2.71	2.69	2.25	2.55	2.74	2.70
Thr[10]	NH	7.56	7.77	7.66	7.81	7.62	7.43	7.75	7.85
	αH	4.00	4.02	4.05	4.11	4.18	4.02	4.14	4.17
	*β*H	3.87	3.89	4.04	3.95	3.91	3.98	4.14	4.05
	*γ*H	0.85	0.85	0.96	0.95	0.98	0.92	1.06	1.06
	OH			5.07	5.02	5.02	5.07	5.09	4.96
		Phe	Phe	Phe	Phe	Phe	Phe	Ala	Ala
Phe/Ala[11]	NH	8.07	8.03	7.78	7.85	8.14	7.95	7.83	7.90
	αH	4.40	4.44	4.57	4.62	4.64	4.54	4.30	4.32
	*β*H	3.16, 2.88	3.10, 2.85	3.08, 2.83	3.05, 2.86	3.09, 2.86	3.08, 2.85	1.25	1.23
	H2,6	7.24	7.25	7.25	7.25	7.29	7.24		
	H3,5	7.17		7.03		7.23	7.18		
	H4								
Cys[14]	NH	7.69	7.90	8.61	8.51	8.22	8.54	8.45	8.33
	αH	4.03	4.11	4.51	4.55	4.46	4.56	4.51	4.05
	*β*H	3.23, 3.13	3.06	3.11, 3.00	3.05, 2.86	3.08, 3.00	3.09, 3.04	3.11, 3.01	3.08, 3.04

[a] The chemical shifts were measured at 293 K in DMSO in ppm, with the internal reference of the DMSO signal at 2.49 ppm.

the sst_2/sst_5-selective (and sst_3) analogues, which is consistent with the missing *β*-turn around these residues (see below).

A large number of experimental NOEs is observed (a representative NOESY spectrum of analogue **7** is shown in Figure 1) for all eight analogues in the NOESY spectrum measured with a mixing time of 100 or 150 ms, leading to over 100 meaningful distance restraints per analogue and concomitantly ∼15 restraints per residue, which is a typical number for folded proteins (Table 3). Interestingly, this large number of NOEs is not observed in the case of sst_1- and sst_3-selective analogues presently under study in our laboratories (unpublished results). Hence, it should be emphasized that the protein-like behavior seen here in the number of observed NOEs is a unique characteristic of this family of sst_4-selective analogues. In contrast, only a few meaningful $^3J_{HN\alpha}$ (region for which an average of multiple conformation in fast exchange cannot be excluded) scalar coupling constants were obtained from 1D ^{1}H NMR experiments, because most of the scalar couplings are in the ambiguous region between 6 and 8 Hz and/or an accurate measurement of the scalar coupling is not possible due to line broadening (Figure 1).

These structural restraints were used as input for the structure calculation with the program CYANA,[32] followed by restrained energy minimization using the program DISCOVER.[33] The resulting bundle of 20 conformers per analogue represents the 3D solution structure of each analogue. For each analogue, the small residual constraint violations in the 20 refined conform-

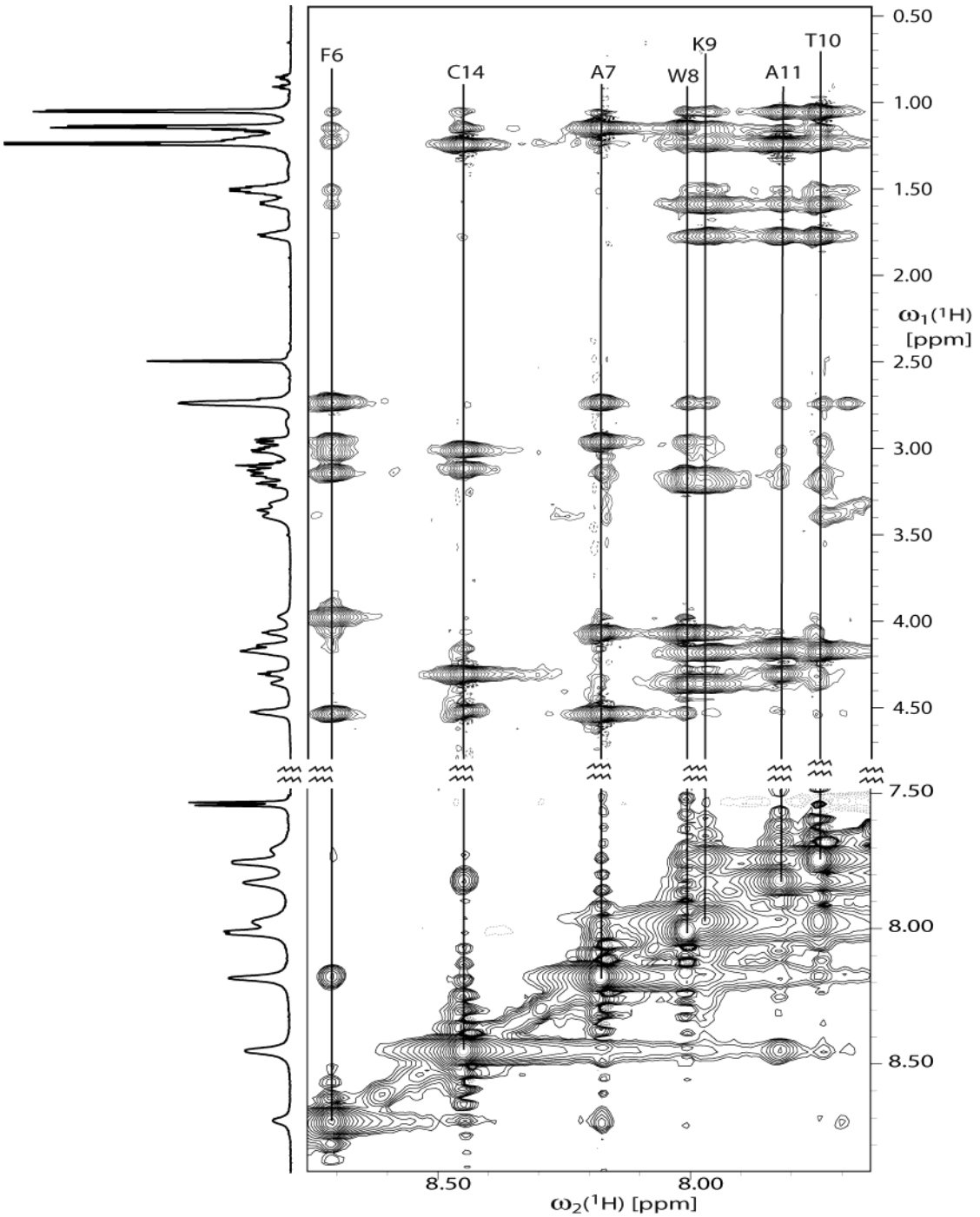

Figure 1. Amide region of the two-dimensional [^{1}H,^{1}H] NOESY spectrum of **7** in DMSO at 293 K. Mixing time is 100 ms, number of scans is 64, with a relaxation delay of 1 s. 800 × 1024 complex data points were acquired, followed by zero-filling to 1024 × 2048 points before Fourier transformation. The amide resonances of the different residues are marked on the spectrum with one-letter codes. The 1D ^{1}H spectrum with eight transients is plotted as a projection. The signal from the residual water in the solvent is suppressed by presaturation during the relaxation delay and mixing time.

ers (Table 3) and the good coincidence of experimental NOEs and short interatomic distances (data not shown) indicate that the input data represent a self-consistent set, and that the restraints are well satisfied in the calculated conformers (Table 3). The deviations from ideal geometry are minimal, and similar energy values were obtained for all 20 conformers of each analogue. The quality of the structures determined is reflected by the small backbone RMSD values relative to the mean coordinates of ~0.5 Å (see Table 3 and Figure 3).

Three-Dimensional Structure of H-c[Cys^3-Phe^6-Phe^7-Trp^8-Lys^9-Thr^{10}-Phe^{11}-Cys^{14}]-OH (1). Analogue **1** binds to all five sst's with high affinity (IC_{50} < 15 nM), with the exception of sst_2 (IC_{50} = 130 nM). The quality of the structure is reflected by the small RMSD (Table 3), which can also be visually depicted from Figure 3, showing the bundle of 20 conformers representing the 3D structure. On the basis of the backbone torsion angles (Table 4), the 3D structure contains two turns, a β-turn of type III around Phe^7-Trp^8 and a β-turn of

Table 3. Characterization of the NMR Structures of Analogues **1**−**8**[a]

									residual restraint violations on			
						CFF91 energies (kcal/mol)			distances		dihedral angles	
no.	NOE distance restraints[c]	angle restraints	CYANA target function[b]	backbone RMSD (Å)	overall RMSD (Å)	total energy	van der Waals	electrostatic	no. ≥0.1 Å	max (Å)	no. ≥1.5°	max (deg)
1	115	20	0.27	0.17 ± 0.08	0.59 ± 0.06	181.3 ± 75.2	26.9 ± 1.4	87.1 ± 2.5	1.7 ± 0.1	0.18 ± 0.0	2.6 ± 0.6	1.99 ± 0.6
2	116	22	0.001	0.65 ± 0.12	1.39 ± 0.21	192.7 ± 18.4	30.2 ± 1.8	100.5 ± 3.4	0.1 ± 0.1	0.04 ± 0.03	0 ± 0	0 ± 0
3	113	27	0.002	0.50 ± 0.14	0.89 ± 0.16	185.3 ± 86.7	32.2 ± 3.2	98.7 ± 4.1	0.3 ± 0.1	0.08 ± 0.02	0.3 ± 0.25	0.2 ± 0.23
4	118	22	0.0005	0.28 ± 0.11	0.70 ± 0.10	165.1 ± 50.7	25.7 ± 1.0	89.4 ± 1.3	0.1 ± 0.0	0.03 ± 0.0	0 ± 0	0 ± 0
5	108	21	0.11	0.47 ± 0.14	0.81 ± 0.12	122.6 ± 192	34.0 ± 1.5	84.5 ± 2.8	0.7 ± 0.1	0.14 ± 0.03	0.9 ± 1.1	0.66 ± 0.68
6	128	15	0.004	0.22 ± 0.07	0.92 ± 0.18	125.2 ± 223	35.0 ± 2.4	83.5 ± 3.1	0.7 ± 0.1	0.09 ± 0	0 ± 0	0 ± 0
7	140	30	0.0067	0.30 ± 0.19	0.64 ± 0.15	190.5 ± 413	28.9 ± 1.2	95.9 ± 2.4	0.3 ± 0.1	0.09 ± 0.03	4.4 ± 1.0	3.0 ± 0.83
8	106	28	0.0033	0.26 ± 0.05	0.56 ± 0.05	172.3 ± 68.4	23.0 ± 0.9	89.9 ± 1.5	0.2 ± 0.1	0.07 ± 0	2.4 ± 0.2	1.45 ± 0.17

[a] The bundle of 20 conformers with the lowest residual target function was used to represent the NMR structures of each analogue. [b] The target function is zero only if all the experimental distance and torsion angle constraints are fulfilled and all nonbonded atom pairs satisfy a check for the absence of steric overlap. The target function is proportional to the sum of the square of the difference between calculated distance and isolated constraint or van der Waals restraints, and similarly isolated angular restraints are included in the target function. For the exact definition, see ref 32. [c] Meaningful NOE distance restraints may include intraresidual and sequential NOEs.[32]

Table 4. Torsion Angles ϕ, ψ, and χ_1 (in deg) of the Bundle of 20 Energy-Minimized Conformers

analogue	angle							
1		Phe^6	Phe^7	Trp^8	Lys^9	Thr^{10}	Phe^{11}	Cys^{14}
	ϕ	−66 ± 3	−61 ± 2	(III) −68 ± 3	66 ± 3	−75 ± 2	(VIII) −120 ± 1	1 ± 3
	ψ	171 ± 4	−48 ± 3	−13 ± 2	0 ± 3	−36 ± 1	47 ± 5	
	χ_1	55 ± 5	−174 ± 2	62 ± 2	−110 ± 33	−55 ± 1	−56 ± 2	−160 ± 32
2		Phe^6	Phe^7	D-Trp^8	Lys^9	Thr^{10}	Phe^{11}	Cys^{14}
	ϕ	−116 ± 9	67 ± 2	(VIII′)138 ± 5	−94 ± 4	105 ± 12	−111 ± 13	77 ± 5
	ψ	159 ± 5	66 ± 1	−45 ± 6	−65 ± 4	−22 ± 3	−42 ± 13	
	χ_1	−38 ± 9	−159 ± 1	58 ± 1	−80 ± 44	−144 ± 3	−132 ± 20	−103 ± 59
3		Phe^6	Ala^7	Trp^8	Lys^9	Thr^{10}	Phe^{11}	Cys^{14}
	ϕ	−75 ± 12	(γ)−71 ± 8	−151 ± 20	(γ)−71 ± 3	55 ± 5	−148 ± 25	18 ± 30
	ψ	172 ± 12	87 ± 7	−152 ± 12	13 ± 16	57 ± 6	−45 ± 19	
	χ	−69 ± 18	179 ± 2	−171 ± 8	68 ± 5	56 ± 35	−165 ± 15	−27 ± 60
4		Phe^6	Ala^7	D-Trp^8	Lys^9	Thr^{10}	Phe^{11}	Cys^{14}
	ϕ	−149 ± 7	−84 ± 1	(II) 70 ± 3	−136 ± 5	−125 ± 3	−71 ± 4	35 ± 34
	ψ	150 ± 3	131 ± 3	18 ± 2	−37 ± 4	143 ± 3	−49 ± 4	
	χ_1	−152 ± 3	−179 ± 1	−66 ± 4	−61 ± 4	69 ± 1	−64 ± 25	−51 ± 83
5		Phe^6	Tyr^7	D-*threo*-β-Me2Nal^8	Lys^9	Thr^{10}	Phe^{11}	Cys^{14}
	ϕ	−101 ± 26	−113 ± 20	44 ± 5	(III′) 50 ± 2	−119 ± 8	−161 ± 8	−86 ± 91
	ψ	158 ± 14	−102 ± 5	42 ± 4	34 ± 6	−61 ± 16	146 ± 37	
	χ_1	55 ± 8	−69 ± 5	−55 ± 3	57 ± 1	−65 ± 2	−172 ± 2	−164 ± 34
6		Phe^6	Tyr^7	L-*threo*-β-Me2Nal^8	Lys^9	Thr^{10}	Phe^{11}	Cys^{14}
	ϕ	−155 ± 55	−114 ± 25	−147 ± 10	−72 ± 8	(III) −66 ± 7	155 ± 13	−134 ± 26
	ψ	59 ± 30	−14 ± 9	172 ± 8	−27 ± 11	−37 ± 6	−66 ± 4	
	χ_1	−151 ± 95	−50 ± 5	−134 ± 28	−49 ± 7	−171 ± 4	164 ± 3	−153 ± 41
7		Phe^6	Ala^7	Trp^8	Lys^9	Thr^{10}	Ala^{11}	Cys^{14}
	ϕ	−116 ± 19	−33 ± 27	(II) 88 ± 1	85 ± 3	54 ± 5	(III′) 83 ± 1	66 ± 46
	ψ	115 ± 31	115 ± 6	−161 ± 1	40 ± 2	42 ± 5	54 ± 12	
	χ_1	−155 ± 6	−149 ± 90	100 ± 1	−132 ± 7	81 ± 6	167 ± 94	−121 ± 88
8		Phe^6	Ala^7	D-Trp^8	Lys^9	Thr^{10}	Ala^{11}	Cys^{14}
	ϕ	−159 ± 2	−60 ± 5	(II) 77 ± 10	−134 ± 0	55 ± 8	(III′) 61 ± 9	−5 ± 56
	ψ	−166 ± 5	152 ± 10	8 ± 3	6 ± 0	24 ± 8	39 ± 26	
	χ	−37 ± 4	−132 ± 99	−76 ± 2	−30 ± 4	−154 ± 21	−146 ± 83	69 ± 30

type VIII around Thr^{10}-Phe^{11}. Both turns are supported by sequential and medium-range backbone NOEs {$d_{\alpha N}(i,i+2)$, $d_{NN}(i,i+2)$} (Figure 2) and by hydrogen bonds Lys^{9}HN-O′Phe^6 and Cys^{14}HN-O′Lys^9 observed in all 20 conformers. The relatively small temperature coefficient observed, −2.6 ppb/K, for the amide protons of Lys^9 and Cys^{14} further supports the β-turn conformation (data not shown). On the basis of the torsion angles listed in Table 4, the side chain of Phe^6 is in the gauche$^-$ rotamer, that of Phe^7 is in the trans rotamer, that of Trp^8 is in the gauche$^-$ rotamer, and those of Lys^9 and Phe^{11} are in the gauche$^+$ rotamer. Concomitantly, the side chains of Trp^8 and Lys^9 are oriented opposite of each other, with the aromatic rings of Phe^6 and Phe^{11} adjacent to the side chain of Trp^8.

Three-Dimensional Structure of H-c[Cys^3-Phe^6-Phe^7-D-Trp^8-Lys^9-Thr^{10}-Phe^{11}-Cys^{14}]-OH (2). Analogue **2** differs from analogue **1** only in the chirality of Trp^8, inducing a different 3D structure (Figure 3). The backbone torsion angles (Table 4) indicate a β-turn of

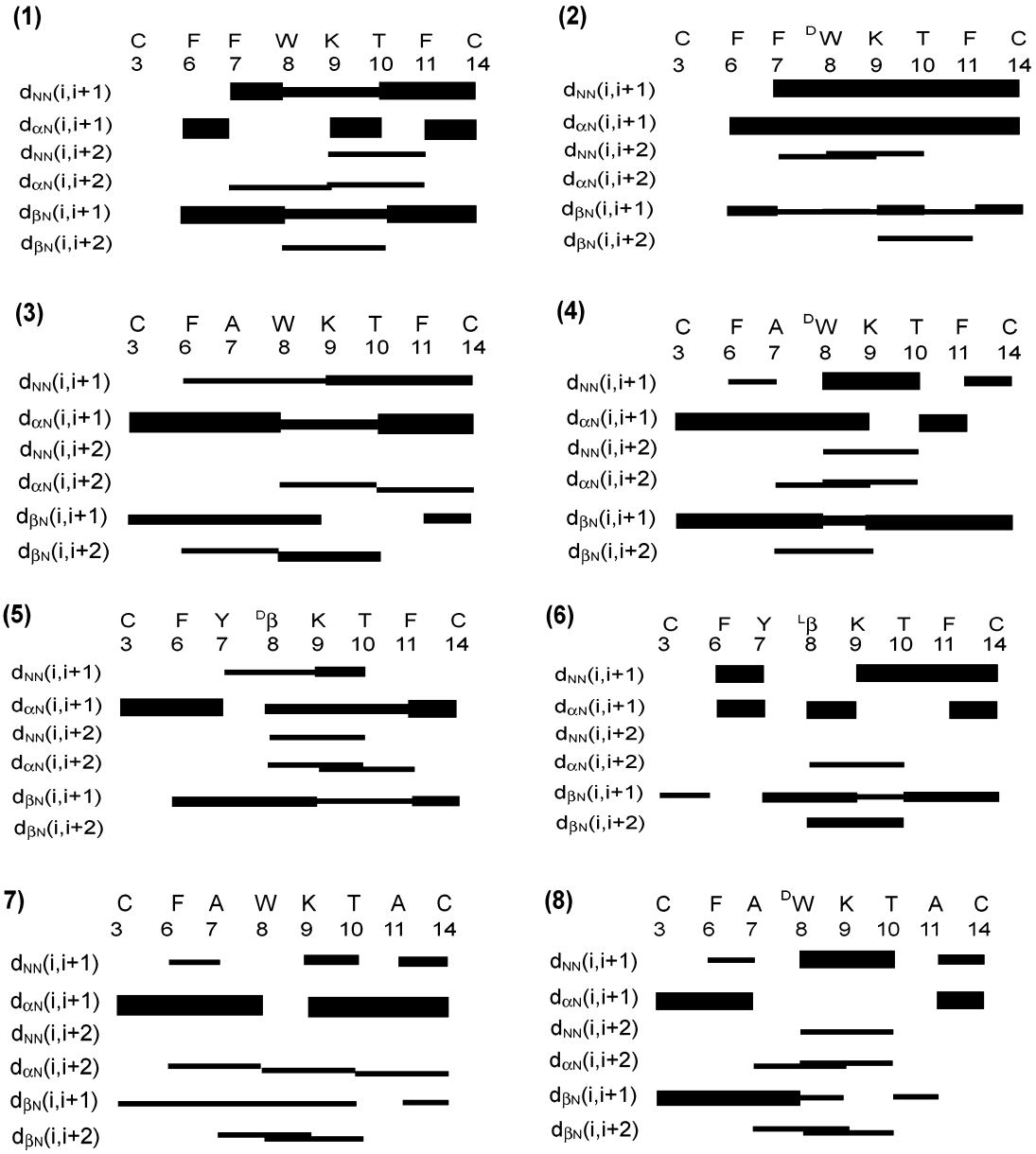

Figure 2. Survey of characteristic NOEs used in CYANA for structure calculation for analogues **1**−**8**. Thin, medium, and thick bars represent weak (4.5−6 Å), medium (3−4.5 Å), and strong (<3 Å) NOEs observed in the NOESY spectrum. The medium-range connectivities, $d_{NN}(i,i+2)$, $d_{\alpha N}(i,i+2)$, and $d_{\beta N}(i,i+2)$ are shown by lines starting and ending at the positions of the residues related by the NOE. Residues designated with "$^{D}\beta$" and "$^{L}\beta$" correspond to the amino acid D-*threo*-β-Me2Nal and L-*threo*-β-Me2Nal, respectively.

type VIII′ conformation around Phe^7-DTrp^8. A turn-like structure is also supported by the medium-range $d_{NN}(i,i+2)$ distance restraints (Figure 2). Although the low-temperature coefficient of 0 ppb/K for the amide proton of Lys^9 is indicative of the expected hydrogen bond Lys^{9}NH-O′Phe^6, the carbonyl C═O of Phe^6 is not in a hydrogen-bond-favorable orientation. The side chain of Phe^6 is in the gauche$^+$ rotamer, that of Phe^7 is in the trans rotamer, that of DTrp^8 is in the gauche$^-$ rotamer, and that of Lys^9 is in the gauche$^+$ rotamer (Table 4). Conclusively, the side chains of DTrp^8 and Phe^7 are adjacent to each other in the plane of the analogue backbone, whereas the side chains of Phe^6 and Phe^{11} are pointing away from the plane of the peptide backbone. The presence of DTrp^8 brings the side chain of Lys^9 closer to the indole ring of DTrp^8, which is observed in the conformations of analogues binding selectively to sst$_2$/sst$_5$ receptors.

Three-Dimensional Structure of H-c[Cys^3-Phe^6-Ala^7-Trp^8-Lys^9-Thr^{10}-Phe^{11}-Cys^{14}]-OH (3). Analogue **3** binds with high affinity and selectively to the sst$_4$ receptor. The chemical structure differs from that of **1** by the replacement of Phe^7 with Ala, which induces a large conformational change. Instead of a β-turn, an inverse γ-turn is observed around Ala^7 and Lys^9, resulting in a nonregular bent structure. The γ-turn is supported by the backbone torsion angles (Table 4) and by the hydrogen bond Trp^{8}HN-O′Phe^6. The low-temperature coefficient of −2.8 ppb/K observed for the amide hydrogen of Trp^8 further supports the hydrogen bond formation. The side chain of Phe^6 is in the gauche$^+$ rotamer, that of Trp^8 is in the trans rotamer, that of

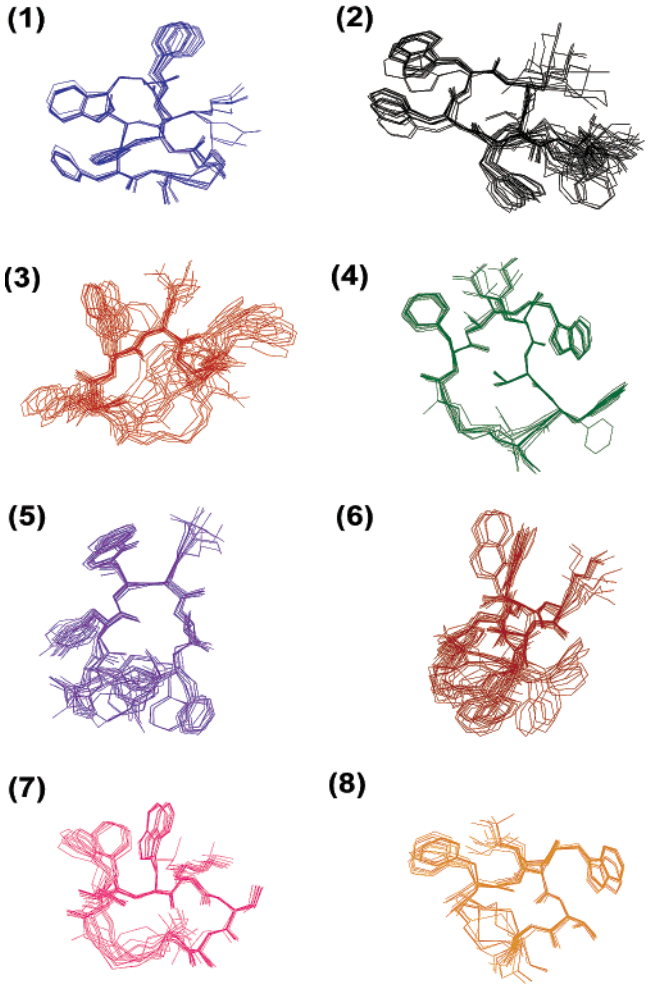

Figure 3. NMR structures of analogues **1**−**8**. For each analogue, 20 energy-minimized conformers with the lowest target function are used to represent the 3D NMR structure. The bundle is obtained by superposition of C^{α} atoms of the residues 2−7. The backbone and all side chains are displayed, including the disulfide bridge. The following color code is used: blue, H-c[Cys-Phe-Phe-Trp-Lys-Thr-Phe-Cys]-OH (**1**), black H-c[Cys-Phe-Phe-D-Trp-Lys-Thr-Phe-Cys]-OH (**2**), red H-c[Cys-Phe-Ala-Trp-Lys-Thr-Phe-Cys]-OH (**3**), green H-c[Cys-Phe-Ala-D-Trp-Lys-Thr-Phe-Cys]-OH (**4**), violet H-c[Cys-Phe-Tyr-D-*threo*-*β*-Me2Nal-Lys-Thr-Phe-Cys]-OH (**5**), brown H-c[Cys-Phe-Tyr-L-*threo*-*β*-Me2Nal-Lys-Thr-Phe-Cys]-OH (**6**), pink H-c[Cys-Phe-Ala-Trp-Lys-Thr-Ala-Cys]-OH (**7**), and orange H-c[Cys-Phe-Ala-D-Trp-Lys-Thr-Ala-Cys]-OH (**8**).

Lys^9 is in the gauche$^-$, rotamer and that of Phe^{11} is in the trans rotamer (Table 4). The resulting relative spatial orientation of the side chains brings Lys^9 close to the indole ring of Trp^8 and to the aromatic ring of Phe^{11} in a "sandwich" manner. The aromatic ring of Phe^6 is pointing in the same direction but is farther away from this triplet of side chains (Figure 4).

Three-Dimensional Structure of H-c[Cys^3-Phe^6-Ala^7-D-Trp^8-Lys^9-Thr^{10}-Phe^{11}-Cys^{14}]-OH (4). Analogue **4** binds selectively with subnanomolar affinity to the sst_4 receptor. It differs from analogue **3** by the chirality of Trp^8, which results in a different 3D structure (Figure 3). The backbone torsion angles indicate a type II β-turn conformation around Ala^7-D-Trp^8 (Table 4), which is supported by the $d_{\alpha N}(i,i+2)$ NOEs observed between Ala^7 and Lys^9 (Figure 2). The expected hydrogen bond Lys^9NH-O′Phe^6 is observed in all 20 conformers and is supported by the low-temperature coefficient of 0 ppb/K for the amide proton of Lys^9. The side chain of Phe^6 is in the trans rotamer, with those of D-Trp^8, Lys^9, and Phe^{11} in the gauche$^+$ rotamers (Table 4). This orients the side chains of D-Trp^8 and Lys^9 in divergent directions, with the aromatic ring of Phe^6 adjacent to Lys^9 (Figure 4).

Three-Dimensional Structure of H-c[Cys^3-Phe^6-Tyr^7-D-*threo*-*β*-Me2Nal^8-Lys^9-Thr^{10}-Phe^{11}-Cys^{14}]-OH (5). Analogue **5** binds nonselectively to all of the receptors except sst_1 and with maximum binding affinity to sst_4 (Table 1). It differs from analogue **2** by Tyr^7 and D-*threo*-*β*-$Me2Nal^8$. This is the only analogue with the characteristic upfield shift of the Lys^9 side-chain protons (Table 2). The backbone has a type III′ β-turn around D-*threo*-*β*-$Me2Nal^8$ and Lys^9, which is supported by the backbone angles (Table 4) and by the presence of the $d_{\alpha N}(i,i+2)$ NOEs observed between D-*threo*-*β*-$Me2Nal^8$ and Thr^{10}. The expected hydrogen bond Thr^{10}-NH-O′Tyr^7 is observed in all 20 conformers representing the NMR structure and is consistent with the observed low-temperature coefficient of −2.2 ppb/K for the amide proton of Thr^{10}. The side chain of Phe^6 is in the gauche$^-$ rotamer, those of Tyr^7 and D-*threo*-*β*-$Me2Nal^8$ are in the gauche$^+$ rotamer, that of Lys^9 is in the gauche$^-$ rotamer, and that of Phe^{11} is in the trans rotamer (Table 4). This orients the side chains of D-*threo*-*β*-$Me2Nal^8$ and Lys^9 adjacent to each other.

Three-Dimensional Structure of H-c[Cys^3-Phe^6-Tyr^7-L-*threo*-*β*-Me2Nal^8-Lys^9-Thr^{10}-Phe^{11}-Cys^{14}]-OH (6). Analogue **6** binds selectively to the sst_4 receptor with high affinity (Table 1). It differs from **5** in the chirality of residue 8, giving rise to a different conformation (Figure 3). The backbone has a type III β-turn around Lys^9 and Thr^{10}, which is supported by the weak $d_{\alpha N}(i,i+2)$ NOE between L-*threo*-*β*-$Me2Nal^8$ and Thr^{10}. This is also consistent with the low-temperature coefficient −2.8 ppb/K observed for the amide proton of L-*threo*-*β*-$Me2Nal^8$ forming a hydrogen bond with the carbonyl oxygen of Phe^{11}. The side chains of Tyr^7 and Lys^9 are in the gauche$^+$ rotamer, and those of L-*threo*-*β*-$Me2Nal^8$ and Phe^{11} are in the trans rotamer (Table 4). The L-*threo*-*β*-$Me2Nal^8$ and Lys^9 are in close proximity (Figure 4).

Three-Dimensional Structure of H-c[Cys^3-Phe^6-Ala^7-Trp^8-Lys^9-Thr^{10}-Ala^{11}-Cys^{14}]-OH (7). Analogue **7** binds selectively to the sst_4 receptor, having higher binding affinity than **8**. It differs from **3** by the replacement of Phe^{11} by Ala. This results in a different backbone conformation for **7** with two turns: a type II β-turn around Ala^7 and Trp^8 and a type III′ β-turn around Thr^{10} and Ala^{11} (Table 4; Figures 3 and 4). The turn structures are supported by $d_{\alpha N}(i,i+2)$ NOEs observed between Phe^6-Trp^8 and Thr^{10}-Cys^{14} (Figure 1). The expected hydrogen bonds are observed between Trp^8NH-O′Phe^6 and Ala^{11}NH-O′Trp^8 and are supported by the small temperature coefficients observed, −1.8 ppb/K for the amide proton of Trp^8 and −1.4 ppb/K for the amide proton of Ala^{11}. The side chain of Phe^6 is in the trans rotamer, that of Trp^8 is in the gauche$^-$ rotamer, and that of Ala^{11} is in the trans rotamer (Table 4), which results in the close proximity of these side chains (Figure 4).

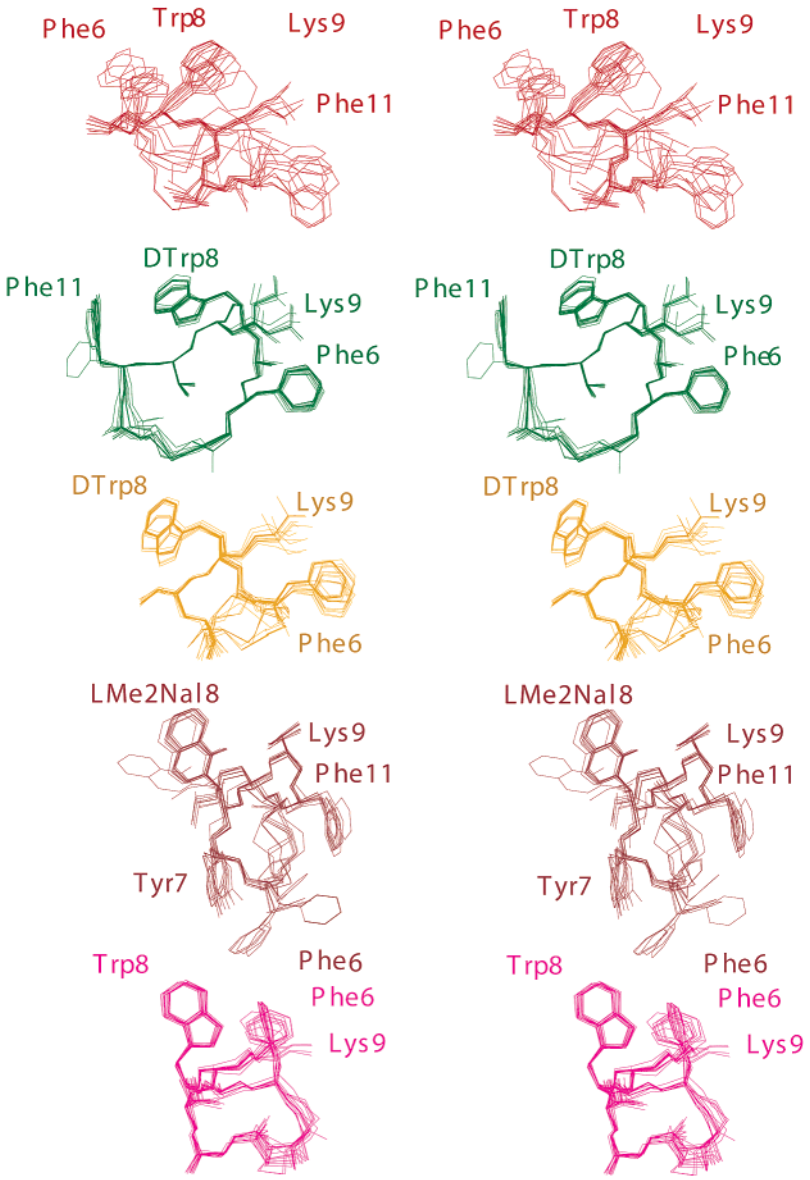

Figure 4. Stereo drawings of the 3D structures of the analogues binding selectively to sst$_4$. The same color code as in Figure 3 is used: red for **3**, green for **4**, orange for **8**, brown for **6**, and pink for **7**. The backbone orientations of the structures are adjusted to indicate that in all of these structures, the side-chain orientations of Trp^8, Lys^9, and Phe^6 or Phe^{11} are similar. Hence, the structures of **4** (green), **8** (orange), and **7** (pink) have been rotated by about 180° when compared with the other structures (see also labeling of the side chains). Some of the side chains are labeled. Though the backbones do not have similar conformation, the side-chain orientations of Trp^8, Lys^9, and Phe^6 or Phe^{11} are similar in these sst$_4$-selective analogues. For each analogue, the 20 energy-minimized conformers with the lowest target function are used to represent the 3D NMR structures. Each bundle is obtained by superposition of C$^\alpha$ atoms of the residues 2−7. The backbone and all side chains are displayed including the disulfide bridge. For analogues **3** and **6**, only 10 energy-minimized conformers are shown in the figure.

Three-Dimensional Structure of H-c[Cys^3-Phe^6-Ala^7-D-Trp^8-Lys^9-Thr^{10}-Ala^{11}-Cys^{14}]-OH (8). Analogue **8** differs from **7** by the chirality of Trp^8 and from **4** by Ala^{11} replacement and binds selectively to the sst$_4$ receptor. The backbone of **8** has two turns, a β-turn of type II around Ala^7 and D-Trp^8 and a β-turn of type III′ around Thr^{10} and Ala^{11} (Table 4; Figures 3 and 4). This is supported by $d_{\alpha N}(i,i+2)$ NOEs observed between Ala^7 and Lys^9, and between D-Trp^8 and Thr^{10} (Figure 2). The hydrogen bonds observed between Lys^{9}NH-O′Phe^6 and Ala^{11}NH-O′Trp^8 are supported by the small temperature coefficients measured, 0 ppb/K for the amide proton of Lys^9 and −0.3 ppb/K for the amide proton of Ala^{11}. The side chains of Phe^6, D-Trp^8, and Lys^9 are in the gauche$^+$ rotamer (Table 4). The side-chain orientations and the backbone conformation are similar to that of **4**, except for the region from Thr^{10} to Cys^{14} as well as the disulfide bridge (Figure 4).

Difficulties in Determining the Conformation of Analogues 9−14. Analogues **9** to **14** were not suitable for NMR structure determination due to the presence of multiple conformations in the NMR spectra. For **9** and **10**, a large number of cross-peaks were observed in 2D experiments, indicating the presence of several conformations. Since both analogues contain a D-Cys^3, the presence of multiple conformations could be due to a slow conformational exchange between *R* and *S* states of the disulfide bond. For **11**−**14**, the 1D ^{1}H NMR spectrum showed two sets of peaks per proton, indicating the presence of two conformers, undergoing confor-

mational exchange slow on the NMR time scale. High-temperature studies indicate the coalescence of this peak to a single resonance. The presence of two conformations could be due to the Agl(N$^{\beta}$Me, benzoyl) residue, which introduces severe constraints on the orientation of the side chain.

Discussion

Our group has synthesized a large number of cyclic octapeptide analogues of SRIF, some of which bind selectively with high affinity to the sst$_4$ receptor.[6−8] Our original goals were to identify highly potent and receptor-selective SRIF analogues to study their tissue distribution, physiological role, mechanism of action, and pharmacology. We show here that the understanding of the structural requirements of cyclic SRIF octapeptides for binding to sst$_4$ derived from extensive structural studies of three peptide families can lead to the proposal of a 3D consensus structure which, in turn, can be used in a predictive manner. In other words, we were able to characterize the bioactive conformation and to elucidate the consensus 3D structural motif of the sst$_4$-selective SRIF analogues **1**−**8** (Table 1) using high-resolution NMR techniques. Assuming that the compounds studied in DMSO are in their bioactive conformation,[23,34] the proposed consensus structure is equivalent to the binding motif of sst$_4$-selective analogues and therefore a pharmacophore for the sst$_4$ receptor.

Three-Dimensional Structures of the Eight Analogues Studied Are Widely Different. Most of the cyclic bioactive analogues of SRIF reported so far have a DTrp at position 8, and the backbone conformation has a predominant β-turn of either type II′ or type VIa.[12,14,16−19,23,25,35−37] Melacini et al. reported that the backbone of sandostatin (octreotide) could be in a conformational equilibrium between β-turn and helical structures in solvents different from DMSO.[30,34] Nonetheless, it is a striking feature of the eight observed structures determined in DMSO that none of them have similar backbone conformations (Figures 3 and 4; Table 4) nor the type II′ β-turn usually observed in cyclic SRIF analogues. The replacement of Trp^8 in **1** with DTrp^8 in **2** changes the backbone conformation (Table 4; Figure 3) from a β-turn of type III around Trp^8 to a β-turn of type VIII′, and concomitantly, the side-chain orientations change dramatically: the side chain of Trp^8 is opposite to the side chain of Lys^9, whereas the side chains of DTrp^8 and Lys^9 are in close proximity. Similarly, the replacement of Phe^7 with Ala changes the backbone conformation from a type III β-turn around Trp^8 to an inverse γ-turn (Table 4; Figure 4). All of the sst$_4$-selective analogues also show different backbone conformations and different 3D structures (Figure 4 and next paragraph). For example, the replacement of Trp^8 in **3** by DTrp in **4** changes the backbone conformation from a γ-turn around Ala^7 to a type II β-turn around Ala^7-DTrp^8. These observations strongly support the idea of Nicolaou et al., who suggested that the analogue backbone is not required for receptor binding but serves as a scaffold for supporting the key side-chain groups.[38]

The Consensus Structural Motif for the sst$_4$-Selective SRIF Analogues. Although the 3D structures among the sst$_4$-selective analogues seem to have minimal resemblance, interestingly they do have similar spatial orientations/location for some of the side chains, suggesting a role for these side chains in enhancing the binding affinity to sst$_4$ receptors as well as disrupting binding to other sst's. Figure 4 shows the stereo drawings of all of the sst$_4$-selective analogues (**3**, **4**, **6**−**8**), oriented individually in a way that supports the importance of the three side chains: the indole at residue 8, the amino-alkyl at Lys^9, and an aromatic ring at either position 6 or 11. As can easily be inferred from Figure 4, the structures of **4**, **7**, and **8** are rotated by ∼180° along the vertical axis, to accomplish a similar side-chain arrangement for the three side chains mentioned previously (Phe^{11} for **3** and **6** or Phe^6 for **4**, **7**, **8**) in all of the 3D structures. The possible replacement of Phe^{11} by Phe^6, resulting in a similar relative partial location of the phenyl ring for both equipotent analogues, was already suggested for cyclic hexapeptides.[14] Initially, we solved the structures of **1**−**6**, and on the basis of these conformers, we proposed to replace Phe^{11} with an Ala in the sst$_4$-selective **3** and **4** in order to further define the role of Phe^6 and Phe^{11}. Comparing the 3D structures of **4** and **8** (green and orange in Figure 4) shows that they have a very similar fold and side-chain arrangement for Trp^8, Lys^9, and Phe^6 and that the most pronounced difference is the lack of the aromatic ring at position 11. Since their biological activities are very similar, this indicates (Table 1) that Phe^{11} is not or is only very weakly involved in the sst$_4$-selective binding, but the relative side-chain orientation of Trp, Lys, and Phe is important. It was expected that **7** would serve as a negative control, since the replacement of Phe^{11} with Ala in **3** (red in Figure 4) would change the proposed binding pocket and should therefore disrupt the binding to the receptor. In contrast, **7** binds with high selectivity and affinity to the sst$_4$ receptor (Table 1). Only the determination of the 3D structure of **7** elucidated the characteristic elements responsible for high selectivity. The backbone conformation of **7** differs largely from that of **3** (Table 4; Figure 4), resulting in a close spatial arrangement of Trp^8, Lys^9, and Phe^6, which resembles the proposed three side chains for sst$_4$-selective SRIF analogues. Therefore, the side chains of Trp^8, Lys^9, and either Phe^6 or Phe^{11} in all of the five sst$_4$-selective analogues are almost at the same position in the binding motif and can be superimposed (Figure 5A), although the backbone conformations are different.

The 3D structures determined for the five sst$_4$-selective SRIF analogues, with widely different backbone conformations, together with the data on bioactivity listed in Table 1 and the preceding papers[6−8] enabled a detailed SAR study. Figure 5B shows the consensus structural motif for the sst$_4$-selective analogues, which consists of the right spatial arrangement of the indole ring, the Lys side chain, and an aromatic ring of a phenylalanine. In this model, the distances between the Cγ of residue 8 and Cγ of Phe is 5.5−9.5 Å, that between Cγ of residue 8 and Cγ of Lys^9 is 4.5−6.5 Å, and that between Cγ of Phe and Cγ of Lys^9 is 4.5−6.5 Å. A better selectivity is obtained when the aromatic ring is in close proximity to the indole and the lysine side chains. Conservative replacements of these residues do not change the binding affinities and receptor selectivity, evidently.[6−8] However, D-*erythro*-β-Me2Nal at position 8 inhibits binding due to the

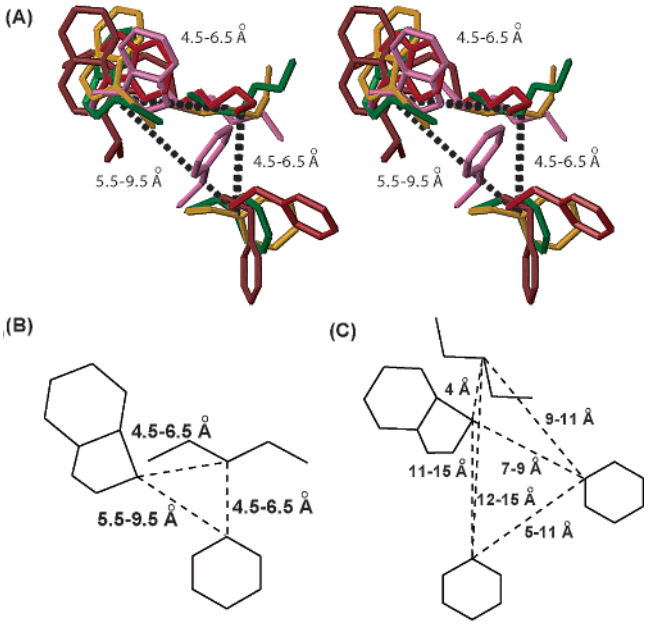

Figure 5. Consensus structural motif of sst$_4$-selective SRIF analogues. (A) Stereoview of the consensus structural motif for the sst$_4$-selective analogues **3** (red), **4** (green), **6** (brown), **8** (orange), and **7** (pink). Only the side chains of residue 8 (Trp, DTrp, or L-*threo*-β-Me2Nal), Lys^9, and Phe^6 for **4**, **7**, and **8** and Phe^{11} for **3** and **6** are shown. The distances between Cγ of residue 8, Cγ of Lys^9, and Cγ of Phe$^{6/11}$ are displayed. For each analogue, the conformer with the lowest target function is displayed. (B) Schematic drawing of the pharmacophore for the sst$_4$-selective SRIF analogues. (C) Schematic drawing of the pharmacophore for the sst$_2$/sst$_5$-selective SRIF analogues.[26]

presence of the methyl group in the β-position, which probably introduces a larger distance between the naphthylalanine and the lysine side chains. Similarly, Phe can be replaced by Tyr, and DTrp can be replaced by D-*threo*-β-Me2Nal or DNal, whereas Lys^9 cannot be replaced by D-Agl(βAla) or D-Agl(N$^{\beta}$Me, βAla).[6] In these analogues, the backbone is not involved in binding and serves only as a scaffold.

Comparison of the sst$_4$-Selective versus sst$_2$/sst$_5$-Selective Pharmacophores. With the introduction of the consensus structural motif for the sst$_4$-selective SRIF analogues (Figure 5A,B), a comparison of this motif with the proposed pharmacophore for sst$_2$/sst$_5$-selective analogues (Figure 5C) is possible. Interestingly, Goodman and co-workers illustrated that in SRIF analogues, which bind selectively to sst$_2$/sst$_5$, the side chains of DTrp^8, Lys^9, and Phe^7 constitute the most essential elements necessary for binding.[25,26] In their pharmacophore model, DTrp^8 and Lys^9 were in close proximity of ~5 Å, but Phe^7 was farther away from DTrp^8 (7−9 Å) and Lys^9 (9−11 Å), which vary from the sst$_4$ pharmacophore, for which a phenylalanine (Phe^6/Phe^{11}) is in close proximity to Trp^8 and Lys^9. This difference can easily be seen in the superposition of the sst$_4$-selective **8** and the sst$_2$/sst$_5$-selective octreotide (Figure 6A).[26] They differ mostly in the position of the phenylalanine ring.

With respect to the two different pharmacophores for sst$_2$/sst$_5$- and sst$_4$-selective analogues, it is interesting to discuss the 3D structures of the nonselective **1**, **2**, and **5**. Analogue **1** binds to sst$_1$, sst$_3$−sst$_5$ with high affinity and to sst$_2$ with low affinity. In contrast, **2** binds to all receptors with high affinity, and **5** binds to all receptors except to sst$_1$ (Table 1). Structural interpretations on analogues with binding affinity to several receptors should be made with caution, since the binding to different receptors might involve an induced-fit mechanism, and therefore the structures determined might change upon binding. However, the intrinsic orientation of the side chains might already be prearranged. Indeed, the structure of **5**, which binds with the highest affinity to sst$_4$ and with a lower affinity to sst$_2$/sst$_3$ and sst$_5$, contains the pharmacophore of both sst$_4$ and sst$_2$/sst$_5$ (Phe^6 or Tyr^7 would be part of the pharmacophore of sst$_2$, and Phe^{11} would be part of the pharmacophore of sst$_4$, Figure 6B). Interestingly, a similar structure containing Phe^7 and Phe^{11} at the corresponding positions in the sst$_2$−sst$_5$ and sst$_4$ pharmacophore is also present in SRIF, which binds with high affinity to all five SRIF receptors.[39] Although in the structure of **2**, the pharmacophore of both sst$_2$/sst$_5$ and sst$_4$ can be found (Phe^7 as part of sst$_2$, Phe^6 or Phe^{11} as part of the pharmacophore of sst$_4$, Figure 6C), the 3D structure of the sst$_2$/sst$_5$-selective analogues differs markedly from that of the sst$_4$-selective analogues (Figure 6A), and a conformational change upon binding to sst$_2$−sst$_5$ must be assumed. It is intriguing to speculate that the large difference observed in the conformation of the nonselective **1** and **2** (Figure 3), when compared with the conformation of all of the sst$_4$-selective analogues (**3**, **4**, **6**−**8**) and the nonselective **5** (which does not bind to sst$_1$), might be important for their binding affinity to sst$_1$. To get further insights in obtaining the consensus structural motif for sst$_1$-selective analogues, further conformational studies must be carried out on such analogues. Another important aspect of the sst$_2$/sst$_5$ and sst$_4$ pharmacophore is the rationale that Phe^7 is important for sst$_2$/sst$_5$ binding, but not for sst$_4$ binding. This observation explains the lower binding affinity to sst$_2$ by replacements at position 7,[6−8] without influencing the binding to sst$_4$, which finally resulted in the development of sst$_4$-selective analogues.

Conclusions

The 3D conformations of eight cyclic SRIF octapeptide analogues having high binding affinity and selectivity to the sst$_4$ receptor have been studied in DMSO. These studies suggest that, although the analogues have different backbone conformations, the relative spatial orientations of the side chains of Yyy,[8] Lys^9, and Phe^6 or Phe^{11} are similar. These studies also indicate that the backbone conformation is not important in binding to the receptor but forms a scaffold to orient the side chains of the essentially important residues, namely indole at position 8, aminoalkyl function at position 9, and an aromatic ring, in their respective positions for effective receptor−ligand binding. On this basis, we propose the SRIF binding motif for the sst$_4$ receptor consisting of these three side chains. This binding motif differs from the binding motif for sst$_2$/sst$_5$-selective receptors in the proximity between the side chains of Lys and Phe (Figure 5). The conformational study of the analogues that bind to all the receptors also confirms the proposed model. Furthermore, the model proposed also explains the selective binding of the non-peptoid analogues of SRIF agonists.[39−42] The elucidation of the

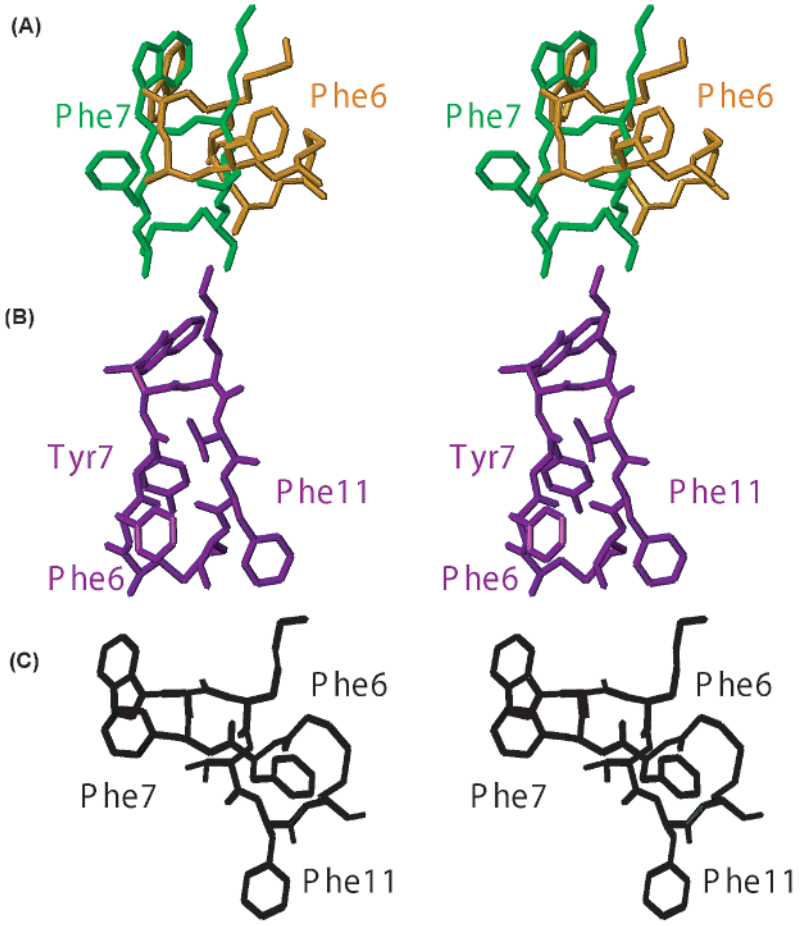

Figure 6. Comparison between the 3D structure of sst_4-selective and sst_2/sst_5-selective SRIF analogues. (A) Stereoview of the superposition of the 3D structure of the sst_4-selective analogue **8** (orange) with the 3D structure of the sst_2/sst_5-selective octreotide (cyan).[26] It must be noted that both phenylalanines labeled are important for selective binding, but they differ in their spatial orientation relative to the DTrp-Lys pair. (B) Stereoview of the 3D structure of **5** (violet), which also binds with high affinity to the sst_2/sst_5 (Table 1). (C) Stereoview of the 3D structure of **2** (black), which binds with high affinity to all five receptors. Analogues **2** and **5** contain the two phenylalanines and one tyrosine important for binding to sst_4 as well as sst_2/sst_5 receptors.

sst_4-selective binding motif and the known motif for sst_2/sst_5-selective analogues support the detailed understanding of SRIF and its receptors and will have an important role in designing highly selective peptide as well as non-peptide ligands of SRIF.

Last, in view of the significant changes in backbone conformation observed as a result of single amino acid substitutions in **3**, **4** and **7**, **8** and seemingly little effect on affinity and selectivity, one may argue in favor of a traditional medicinal chemistry approach to the design of optimized ligands for SRIF receptors. This is best exemplified by results presented in the preceding three papers[6−8] prior to upholding a structure/hypothesis-driven approach that led to **7**.

Experimental Section

Abbreviations. Agl, aminoglycine; CYANA, combined assignment and dynamics algorithm for NMR applications; D-*threo*-*β*-Me2Nal, D-*threo*-*β*-methyl-3-(2-naphthyl)alanine; DMSO, dimethyl sulfoxide; DQF−COSY, double-quantum-filtered correlation spectroscopy; L-*threo*-*β*-Me2Nal, L-*threo*-*β*-methyl-3-(2-naphthyl)alanine; Nal, 3-(2-naphthyl)alanine; NMR, nuclear magnetic resonance; NOESY, nuclear Overhauser enhancement spectroscopy; 3D, three-dimensional; PROSA, processing algorithms; RMSD, root-mean-square deviation; SAR, structure−activity relationship; SRIF, somatostatin; TOCSY, total correlation spectroscopy.

Sample Preparation and NMR Experiments. Analogues were synthesized by the solid-phase approach, either manually or on a CS-Bio peptide synthesizer, model CS536.[6−8] Physicochemical properties of **7** and **8** are as follows: purity >98% by HPLC and CZE using conditions reported earlier.[6] The observed monoisotopic $(M + H)^+$ values of 927.28 and 927.32, for **7** and **8**, respectively, correspond to the calculated $(M + H)^+$ value (927.39) for both peptides.

NMR samples were prepared by dissolving 2.5 mg of the analogue in 0.5 mL of DMSO-d_6. The ^{1}H NMR spectra were recorded on a Bruker 700-MHz spectrometer operating at proton frequency of 700 MHz. Chemical shifts were measured using DMSO ($\delta = 2.49$ ppm) as an internal standard. The 1D spectra were also acquired at temperatures between 293 and 320 K and were used to measure the temperature coefficients of the amide resonances. The 2D spectra were acquired at 293 K. Resonance assignments of the various proton resonances have been carried out using TOCSY,[43,44] DQF−COSY,[45] and NOESY.[46−48] The TOCSY experiments employed the MLEV-17 spin-locking sequence suggested by Davis and Bax,[43] applied for a mixing time of 50 or 70 ms. The NOESY experiments were carried out with a mixing time of 100 or 150 ms. The TOCSY and NOESY spectra were acquired using 800 complex data points in the ω_1 dimension and 1024 complex data points in the ω_2 dimension, with $t_{1max} = 47$ ms and a $t_{2max} = 120$ ms, and were subsequently zero-filled to 1024 × 2048 before Fourier transformation. The DQF−COSY spectra were acquired with 1024 × 4096 data points and were zero-filled to 2048 × 4096 before Fourier transformation. The

TOCSY, DQF−COSY, and NOESY spectra were acquired with 16, 16, and 64 scans, respectively, with a relaxation delay of 1 s. The signal from the residual water of the solvent was suppressed using presaturation during the relaxation delay and during the mixing time. The TOCSY and NOESY data were multiplied by a 75°-shifted sine function in both dimensions. All spectra were processed using the software PROSA.[49] The spectra were analyzed using the software X-EASY.[50]

Structure Determination. The chemical shift assignment of the major conformer (the population of the minor conformer was <10%) was obtained by the standard procedure using DQF−COSY and TOCSY spectra for intra-residual assignment, and the NOESY spectrum was used for the sequential assignment.[51] The collection of structural restraints is based on the NOEs and vicinal $^3J_{NH\alpha}$ couplings. Dihedral angle constraints were obtained from the $^3J_{NH\alpha}$ couplings, which were measured from the 1D ^{1}H NMR spectra and from the intra-residual and sequential NOEs, along with the macro GRIDSEARCH in the program CYANA.[32] The calibration of NOE intensities versus ^{1}H−^{1}H distance restraints and appropriate pseudo-atom corrections to the nonstereospecifically assigned methylene, methyl, and ring protons were performed using the program CYANA. On average, approximately 100 NOE constraints and 20 angle constraints were utilized while calculating the conformers (Table 3). A total of 100 conformers were initially generated by CYANA, and a bundle containing 20 CYANA conformers with the lowest target function values were utilized for further restrained energy minimization, using the CFF91 force field[52] with the energy criteria fit 0.1 kcal mol^{-1} Å^{-1} [53] in the program DISCOVER with conjugate gradients algorithm,[54] as described by Koerber et al.[53] The resulting energy-minimized bundle of 20 conformers was used as a basis for discussing the solution conformation of the different SRIF analogues. The structures were analyzed using the program MOLMOL.[55]

Acknowledgment. This work was supported in part by NIH Grants DK-50124 and DK-59953. We thank Drs. D. Hoyer, T. Reisine, and S. Schulz for the gift of sst$_{1-5}$-transfected CHO-K1, CCL39, and HEK293 cells. We thank Dr. W. Fisher and W. Low for mass spectrometric analyses, and R. Kaiser, C. Miller, and B. Waser for technical assistance in the synthesis and characterization of some peptides and biological testing. We are indebted to D. Doan for manuscript preparation. J.R. is the Dr. Frederik Paulsen Chair in Neurosciences Professor. We thank the H. and J. Weinberg Foundation, the H.N. and F.C. Berger Foundation, and the Auen Foundation for financial support. R.R. is the Pioneer Fund Development Chair.

References

(1) Reichlin, S. Somatostatin. *N. Engl. J. Med.* **1983**, *309*, 1495−1501.
(2) Reichlin, S. Somatostatin (second of two parts). *N. Engl. J. Med.* **1983**, *309*, 1556−1563.
(3) Delfs, J. R.; Dichter, M. A. Effects of somatostatin on mammalian cortical neurons in culture: physiological actions and unusual dose response characteristics. *J. Neurosci.* **1983**, *3*, 1176−88.
(4) Iversen, L. L. Nonopioid neuropeptides in mammalian CNS. *Annu. Rev. Pharmacol. Toxicol.* **1983**, *23*, 1−27.
(5) Patel, Y. C.; Wheatley, T. In vivo and in vitro plasma disappearance and metabolism of somatostatin-28 and somatostatin-14 in the rat. *Endocrinology* **1983**, *112*, 220−225.
(6) Rivier, J.; Erchegyi, J.; Hoeger, C.; Miller, C.; Low, W.; Wenger, S.; Waser, B.; Schaer, J.-C.; Reubi, J. C. Novel sst$_4$-selective somatostatin (SRIF) agonists. 1. Lead identification using a betide scan. *J. Med. Chem.* **2003**, *46*, 5579−5586 (in this issue).
(7) Erchegyi, J.; Penke, B.; Simon, L.; Michaelson, S.; Wenger, S.; Waser, B.; Cescato, R.; Schaer, J.-C.; Reubi, J. C.; Rivier, J. Novel sst$_4$-selective somatostatin (SRIF) agonists. 2. Analogues with *β*-methyl-3-(2-naphthyl)alanine substitutions at position 8. *J. Med. Chem.* **2003**, *46*, 5587−5596 (in this issue).
(8) Erchegyi, J.; Waser, B.; Schaer, J.-C.; Cescato, R.; Rivier, J.; Reubi, J. C. Novel sst$_4$-selective somatostatin (SRIF) agonists. 3. Analogues amenable to radiolabeling. *J. Med. Chem.* **2003**, *46*, 5597−5605 (in this issue).
(9) Lewis, I.; Bauer, W.; Albert, R.; Chandramouli, N.; Pless, J.; Weckbecker, G.; Bruns, C. A novel somatostatin mimic with broad somatotropin release inhibitory factor receptor binding and superior therapeutic potential. *J. Med. Chem.* **2003**, *46*, 2334−2344.
(10) Vale, W.; Rivier, C.; Brown, M.; Rivier, J. Pharmacology of TRF, LRF and somatostatin. *Hypothalamic Peptide Hormones and Pituitary Regulation: Advances in Experimental Medicine and Biology*; Plenum Press: New York, 1977; pp 123−156.
(11) Vale, W.; Rivier, J.; Ling, N.; Brown, M. Biologic and immunologic activities and applications of somatostatin analogs. *Metabolism* **1978**, *27*, 1391−1401.
(12) Veber, D. F.; Freidinger, R. M.; Perlow, D. S.; Paleveda, W. J., Jr.; Holly, F. W.; Strachan, R. G.; Nutt, R. F.; Arison, B. H.; Homnick, C.; Randall, W. C.; Glitzer, M. S.; Saperstein, R.; Hirschmann, R. A potent cyclic hexapeptide analogue of somatostatin. *Nature (London)* **1981**, *292*, 55−58.
(13) Pohl, E.; Heine, A.; Sheldrick, G. M.; Dauter, Z.; Wilson, K. S.; Kallen, J.; Huber, W.; Pfaffli, P. J. Structure of octreotide, a somatostatin analogue. *Acta Crystallogr.* **1995**, *51*, 48−59.
(14) Veber, D. F. Design and discovery in the development of peptide analogs. *Peptides: Chemistry and Biology*, Proceedings of the 12th American Peptide Symposium, Cambridge, MA, June 16−21, 1991; Smith, J. A., Rivier, J. E., Eds.; ESCOM: Leiden, 1992; pp 1−14.
(15) Kessler, H.; Klein, M.; Wagner, K. Peptide conformation. 48. Conformation and biological activity of proline containing cyclic retro-analogues of somatostatin. *Int. J. Pept. Protein Res.* **1988**, *31*, 481−498.
(16) Mierke, D. F.; Pattaroni, C.; Delaet, N.; Toy, A.; Goodman, M.; Tancredi, T.; Motta, A.; Temussi, P. A.; Moroder, L.; Bovermann, G.; Wünsch, E. Cyclic hexapeptides related to somatostatin. *Int. J. Pept. Protein Res.* **1990**, *36*, 418−432.
(17) Huang, A.; Pröbstl, A.; Spencer, J. R.; Yamazaki, T.; Goodman, M. Cyclic hexapeptide analogs of somatostatin containing bridge modifications. *Int. J. Pept. Protein Res.* **1993**, *42*, 352−365.
(18) Mattern, R.-H.; Tran, T.-A.; Goodman, M. Conformational analyses by ^{1}H NMR and computer simulations of cyclic hexapeptides related to somatostatin containing acidic and basic peptoid residues. *J. Pept. Res.* **1999**, *53*, 146−160.
(19) Mattern, R. H.; Tran, T. A.; Goodman, M. Conformational analyses of cyclic hexapeptide analogs of somatostatin containing arylalkyl peptoid and naphthylalanine residues. *J. Pept. Sci.* **1999**, *5*, 161−175.
(20) Jaspers, H.; Horváth, A.; Mezö, I.; Kéri, G.; Van Binst, G. Conformational study of a series of somatostatin analogues with antitumor and/or GH inhibitory activity. *Int. J. Pept. Protein Res.* **1994**, *43*, 271−276.
(21) Hennig, P.; Raimbaud, E.; Thurieau, C.; Volland, J.-P.; Michel, A.; Fauchere, J.-L. Solution conformation by NMR and molecular modeling of three sulfide-free somatostatin octapeptide analogs compared to angiopeptin. *J. Comput.-Aided Mol. Des.* **1996**, *10*, 83−86.
(22) Gilon, C.; Huenges, M.; Mathä, B.; Gellerman, G.; Hornik, V.; Afargan, M.; Amitay, O.; Ziv, O.; Feller, E.; Gamliel, A.; Shohat, D.; Wanger, M.; Arad, O.; Kessler, H. A backbone-cyclic, receptor 5-selective somatostatin analogue: Synthesis, bioactivity, and nuclear magnetic resonance conformational analysis. *J. Med. Chem.* **1998**, *41*, 919−929.
(23) Falb, E.; Salitra, Y.; Yechezkel, T.; Bracha, M.; Litman, P.; Olender, R.; Rosenfeld, R.; Senderowitz, H.; Jiang, S.; Goodman, M. A bicyclic and hsst2 selective somatostatin analogue: design, synthesis, conformational analysis and binding. *Bioorg. Med. Chem.* **2001**, *9*, 3255−3264.
(24) Cheng, R. P.; Suich, D. J.; Cheng, H.; Roder, H.; DeGrado, W. F. Template-constrained somatostatin analogues: a biphenyl linker induces a type-V′ turn. *J. Am. Chem. Soc.* **2001**, *123*, 12710−12711.
(25) Huang, Z.; He, Y.; Raynor, K.; Tallent, M.; Reisine, T.; Goodman, M. Side chain chiral methylated somatostatin analog synthesis and conformational analysis. *J. Am. Chem. Soc.* **1992**, *114*, 9390−9401.
(26) Melacini, G.; Zhu, Q.; Osapay, G.; Goodman, M. A refined model for the somatostatin pharmacophore: Conformational analysis of lanthionine-sandostatin analogs. *J. Med. Chem.* **1997**, *40*, 2252−2258.
(27) Wynants, C.; Van Binst, G.; Loosli, H. R. SMS 201−995, a very potent analogue of somatostatin. Assignment of the ^{1}H 500 MHz nmr spectra and conformational analysis in aqueous solution. *Int. J. Pept. Protein Res.* **1985**, *25*, 608−614.
(28) Kessler, H.; Haupt, A.; Schudok, M.; Ziegler, K.; Frimmer, M. Peptide conformations. 49(1): synthesis and structure−activity relationships of side chain modified peptides of cyclo(-D-Pro-Phe-Thr-Lys-Trp-Phe-). *Int. J. Pept. Protein Res.* **1988**, *32*, 183−193.

(29) He, Y.-B.; Huang, Z.; Raynor, K.; Reisine, T.; Goodman, M. Syntheses and conformations of somatostatin-related cyclic hexapeptides incorporating specific alpha and beta-methylated residues. *J. Am. Chem. Soc.* **1993**, *115*, 8066−8072.
(30) Mattern, R.-H.; Zhang, L.; Rueter, J. K.; Goodman, M. Conformational analyses of sandostatin analogs containing stereochemical changes in positions 6 or 8. *Biopolymers* **2000**, *53*, 506−522.
(31) Jiang, S.; Gazal, S.; Gelerman, G.; Ziv, O.; Karpov, O.; Litman, P.; Bracha, M.; Afargan, M.; Gilon, C.; Goodman, M. A bioactive somatostatin analog without a type II′ beta-turn: synthesis and conformational analysis in solution. *J. Pept. Sci.* **2001**, *7*, 521−528.
(32) Güntert, P.; Mumenthaler, C.; Wüthrich, K. Torsion angle dynamics for NMR structure calculation with the new program DYANA. *J. Mol. Biol.* **1997**, *273*, 283−298.
(33) Hagler, A. T.; Dauber, P.; Osguthorpe, D. J.; Hempel, J. C. Dynamics and conformational energetics of a peptide hormone: vasopressin. *Science* **1985**, *227*, 1309−1315.
(34) Melacini, G.; Zhu, Q.; Goodman, M. Multiconformational NMR analysis of sandostatin (octreotide): Equilibrium between β-sheet and partially helical structures. *Biochemistry* **1997**, *36*, 1233−1241.
(35) Arison, B. H.; Hirschmann, R.; Veber, D. F. Inferences about the conformation of somatostatin at a biologic receptor based on NMR studies. *Biorg. Chem.* **1978**, *7*.
(36) Kessler, H.; Griesinger, C.; Lautz, J.; Muller, A.; van Gunsteren, W. F.; Berendsen, H. J. C. Conformational dynamics detected by nuclear magnetic resonance NOE values and J coupling constants. *J. Am. Chem. Soc.* **1988**, *110*, 3393−3396.
(37) Mattern, R.-H.; Tran, T.-A.; Goodman, M. Conformational analyses of somatostatin-related cyclic hexapeptides containing peptoid residues. *J. Med. Chem.* **1998**, *41*, 2686−2692.
(38) Nicolaou, K. C.; Salvino, J. M.; Raynor, K.; Pietranico, S.; Reisine, T.; Freidinger, R. M.; Hirschmann, R. Design and synthesis of a peptidomimetic employing β-D-glucose for scaffolding. *Peptides: Chemistry, Structure and Biology*; Proceedings of the 11th American Peptide Symposium, La Jolla, CA, July 9−14, 1989; Rivier, J. E., Marshall, G. R., Eds.; ESCOM Science Publishers B.V.: Leiden, The Netherlands, 1990; pp 881−884.
(39) Prasad, V.; Birzin, E. T.; McVaugh, C. T.; Van Rijn, R. D.; Rohrer, S. P.; Chicchi, G.; Underwood, D. J.; Thornton, E. R.; Smith, A. B., III; Hirschmann, R. Effects of heterocyclic aromatic substituents on binding affinities at two distinct sites of somatostatin receptors. Correlation with the electrostatic potential of the substituents. *J. Med. Chem.* **2003**, *46*, 1858−1869.
(40) Ankersen, M.; Crider, M.; Liu, S.; Ho, B.; Andersen, H. S.; Stidsen, C. Discovery of a novel non-peptide somatostatin agonist with SST4 selectivity. *J. Am. Chem. Soc.* **1998**, *120*, 1368−1373.
(41) Liu, S.; Tang, C.; Ho, B.; Ankersen, M.; Stidsen, C. E.; Crider, A. M. Nonpeptide somatostatin agonists with sst_4 selectivity: Synthesis and structure−activity relationships of thioureas. *J. Med. Chem.* **1998**, *41*, 4693−4705.
(42) Rohrer, S. P.; Birzin, E. T.; Mosley, R. T.; Berk, S. C.; Hutchins, S. M.; Shen, D.-M.; Xiong, Y.; Hayes, E. C.; Parmar, R. M.; Foor, F.; Mitra, S. W.; Degrado, S. J.; Shu, M.; Klopp, J. M.; Cai, S.-J.; Blake, A.; Chan, W. W. S.; Pasternak, A.; Yang, L.; Patchett, A. A.; Smith, R. G.; Chapman, K. T.; Schaeffer, J. M. Rapid identification of subtype-selective agonists of the somatostatin receptor through combinatorial chemistry. *Science* **1998**, *282*, 737−740.
(43) Davis, D. G.; Bax, A. Assignment of complex ^{1}H NMR spectra via two-dimensional homonuclear Hartmann−Hahn spectroscopy. *J. Am. Chem. Soc.* **1985**, *107*, 2820−2821.
(44) Braunschweiler, L.; Ernst, R. R. Coherence transfer by isotropic mixing: Application to proton correlation spectroscopy. *J. Magn. Reson.* **1983**, *53*, 521−528.
(45) Rance, M.; Sorensen, O. W.; Bodenhausen, B.; Wagner, G.; Ernst, R. R.; Wüthrich, K. Improved spectral resolution in COSY1H NMR spectra of proteins via double quantum filtering. *Biochem. Biophys. Res. Commun.* **1983**, *117*, 479−485.
(46) Kumar, A.; Wagner, G.; Ernst, R. R.; Wüthrich, K. Buildup rates of the nuclear Overhauser effect measured by two-dimensional proton magnetic resonance spectroscopy: Implications for studies of protein conformation. *J. Am. Chem. Soc.* **1981**, *103*, 3654−3658.
(47) Macura, S.; Ernst, R. R. Elucidation of cross-relaxation in liquids by two-dimensional NMR spectroscopy. *Mol. Phys.* **1980**, *41*, 95−117.
(48) Macura, S.; Huang, Y.; Suter, D.; Ernst, R. R. Two-dimensional chemical exchange and cross-relaxation spectroscopy of coupled nuclear spins. *J. Magn. Reson.* **1981**, *43*, 259−281.
(49) Güntert, P.; Dotsch, V.; Wider, G.; Wüthrich, K. Processing of multi-dimensional NMR data with the new software PROSA. *J. Biolmol. NMR* **1992**, *2*, 619−629.
(50) Eccles, C.; Güntert, P.; Billeter, M.; Wüthrich, K. Efficient analysis of protein 2D NMR spectra using the software package EASY. *J. Biomol. NMR* **1991**, *1*, 111−130.
(51) Wüthrich, K. *NMR of Proteins and Nucleic Acids*; J. Wiley & Sons: New York, 1986.
(52) Maple, J. R.; Thacher, T. S.; Dinur, U.; Hagler, A. T. Biosym force field research results in new techniques for the extraction of inter- and intramolecular forces. *Chem. Design Autom. News* **1990**, *5*, 5−10.
(53) Koerber, S. C.; Rizo, J.; Struthers, R. S.; Rivier, J. E. Consensus bioactive conformation of cyclic GnRH antagonists defined by NMR and molecular modeling. *J. Med. Chem.* **2000**, *43*, 819−828.
(54) Hagler, A. T. Theoretical simulation of conformation, energetics and dynamics of peptides. *Peptides: Analysis, Synthesis, Biology*; Academic Press: Orlando, FL, 1985; pp 213−299.
(55) Koradi, R.; Billeter, M. MOLMOL: a program for display and analysis of macromolecular structures. *PDB Newsl.* **1998**, *84*, 5−7.

JM030246P